Quasi-Static and Dynamic Analysis of Composite Panels: Characterization and Validation

Paria Naghipour Ghezeljeh
Ohio Aerospace Institute, Brook Park, Ohio

Steven M. Arnold, Bradley A. Lerch, Gary D. Robert, Joseph M. Pereira, and Charles R. Ruggeri
Glenn Research Center, Cleveland, Ohio

NASA STI Program . . . in Profile

Since its founding, NASA has been dedicated to the advancement of aeronautics and space science. The NASA Scientific and Technical Information (STI) Program plays a key part in helping NASA maintain this important role.

The NASA STI Program operates under the auspices of the Agency Chief Information Officer. It collects, organizes, provides for archiving, and disseminates NASA's STI. The NASA STI Program provides access to the NASA Technical Report Server—Registered (NTRS Reg) and NASA Technical Report Server— Public (NTRS) thus providing one of the largest collections of aeronautical and space science STI in the world. Results are published in both non-NASA channels and by NASA in the NASA STI Report Series, which includes the following report types:

- TECHNICAL PUBLICATION. Reports of completed research or a major significant phase of research that present the results of NASA programs and include extensive data or theoretical analysis. Includes compilations of significant scientific and technical data and information deemed to be of continuing reference value. NASA counter-part of peer-reviewed formal professional papers, but has less stringent limitations on manuscript length and extent of graphic presentations.

- TECHNICAL MEMORANDUM. Scientific and technical findings that are preliminary or of specialized interest, e.g., "quick-release" reports, working papers, and bibliographies that contain minimal annotation. Does not contain extensive analysis.

- CONTRACTOR REPORT. Scientific and technical findings by NASA-sponsored contractors and grantees.

- CONFERENCE PUBLICATION. Collected papers from scientific and technical conferences, symposia, seminars, or other meetings sponsored or co-sponsored by NASA.

- SPECIAL PUBLICATION. Scientific, technical, or historical information from NASA programs, projects, and missions, often concerned with subjects having substantial public interest.

- TECHNICAL TRANSLATION. English-language translations of foreign scientific and technical material pertinent to NASA's mission.

For more information about the NASA STI program, see the following:

- Access the NASA STI program home page at http://www.sti.nasa.gov

- E-mail your question to help@sti.nasa.gov

- Fax your question to the NASA STI Information Desk at 757-864-6500

- Telephone the NASA STI Information Desk at 757-864-9658

- Write to:
  NASA STI Program
  Mail Stop 148
  NASA Langley Research Center
  Hampton, VA 23681-2199

NASA/TM—2019-220350

Quasi-Static and Dynamic Analysis of Composite Panels: Characterization and Validation

Paria Naghipour Ghezeljeh
Ohio Aerospace Institute, Brook Park, Ohio

Steven M. Arnold, Bradley A. Lerch, Gary D. Robert, Joseph M. Pereira, and Charles R. Ruggeri
Glenn Research Center, Cleveland, Ohio

Acknowledgments

Level of Review: This material has been technically reviewed by technical management.

Quasi-Static and Dynamic Analysis of Composite Panels: Characterization and Validation

Paria Naghipour Ghezeljeh
Ohio Aerospace Institute
Brook Park, Ohio 44142

Steven M. Arnold, Bradley A. Lerch, Gary D. Robert, Joseph M. Pereira, and Charles R. Ruggeri
National Aeronautics and Space Administration
Glenn Research Center
Cleveland, Ohio 44135

Abstract

The predictive capability of a progressive damage model to simulate the quasi-static and dynamic crushing of composite specimens is evaluated in this article. The material model is commercially available within the ABAQUS finite element software package, i.e., "Damage for Fiber reinforced Composites", and is often utilized to simulate damage progression and failure in static and dynamic failure scenarios such as crushing of a composite plate. The composite specimens used in this study consist of quasi-isotropic C-shaped and corrugated composite panels comprised of carbon fiber/epoxy braided fabric. The C-shaped panel specimen is used to calibrate the model and optimize material/model properties through comparison with experimental results. Then, using the same model parameters, the quasi-static crush response of the corrugated panel is predicted. The predictive capability of the model is further demonstrated by simulating the dynamic crushing response of both C-shaped and corrugated panels using the same material properties as in the quasi-static crush case with only minor adjustments for the dynamic elastic properties (i.e., rate dependent modulus). Results show that the in-built material model available in ABAQUS can successfully reproduce experimental results for both panels (C-shaped and corrugated) subjected to both quasi-static and dynamic loading scenarios. A small-scale parametric study on physical (experimentally measurable) and nonphysical (purely mathematical) model parameters was also conducted. It can be concluded that, achieving successful simulation results requires a more in-depth understanding of the influence of model parameter variation on the mechanical response of the composite together with the strategies and challenges of the utilized modeling methodology (e.g., FEA mesh density, etc.).

Introduction

A reliable numerical model that addresses the crushing response of composite materials requires a nonlinear analysis including progressive damage and failure, which makes it a particularly challenging task as an engineering-level analysis. Interaction of several failure mechanisms, such as matrix cracking, fragmentation, delamination, fiber tensile fracture and compressive kinking leads to progressive crushing and failure of a composite panel (Refs. 1 and 2). One might be able to address all these failure responses in a research-based project with no time limits, however, capturing all of these failure mechanisms in a single analysis requires extensive computational power and is not efficient as an engineering approach. In engineering applications, where analysis time and efficiency is essential, analytical models and commercially available finite element (FE) material models are the two mainstream methods used to analyze composite crush scenarios. Hinton et al. (Ref. 3), present a detailed summary of analytical models

based on lamina-level failure criteria that have been used to predict the onset of damage using laminate codes with their specific limitations. In most of the analytical models an orthotropic linear elastic material definition is assumed for the composite with a given failure criterion and a defined failure surface. Beyond the failure surface, a simple degradation scheme is occasionally used to degrade elastic properties. However, these analytical methods rely on numerous empirical approximations and the progressive crushing behavior of a composite after damage initiation is not fully addressed (Ref. 3).

Commercially available codes with built-in material models, which are generally used by the engineering community to analyze crushing behavior of composites, include LS-DYNA, ABAQUS Explicit, RADIOSS and PAM-CRASH (Ref. 4). These built-in material models have some similarities such as utilizing damage initiation, damage propagation, and failure criteria based on physical (experimentally measurable) material properties. However, every material model is implemented differently and accompanied by some nonphysical model parameters, which cannot be measured experimentally. These parameters often times have an important impact on simulation accuracy, and therefore understanding their influence is crucial to developing a reliable and predictive numerical model for composite crushing.

Conducting a parametric study on physical and nonphysical model parameters is essential to understanding the effect of these properties on load-displacement response and crush patterns of a given composite panel configuration. A robust built-in material model should be able to reproduce experimental results reasonably well without the need to extensively modify model parameters for each different composite geometry (shape and layup) or model discretization. It also enables the user to determine an optimized set of properties to produce reasonably acceptable results irrespective of composite geometry.

There are several works available in the literature addressing the crush response of composite panels with different geometries; utilizing the built-in composite material models in commercially available FE codes (Refs. 5 to 15). However, the influence of variations in model parameters and material properties on the crushing behavior of composite specimens is rarely addressed. Among the studies addressing the effect of model parameters on crush response of a composite are the works of Littell et al. (Ref. 13), Feraboli et al. (Ref. 14), and Wade et al. (Ref. 15). Littell et al. (Ref. 13) developed two composite energy absorbers (in conusoid and sinusoid forms) to be evaluated experimentally and numerically through crush tests at NASA Langley Research Center as a part of a larger impact program. The material model used in their study was MAT58 in LS-DYNA, which is a continuum damage mechanics material model used for representing composite laminates and fabrics (Ref. 16). Although crush simulation results in LS-DYNA showed excellent comparison with crush test data, the two geometries were separately calibrated based on individual experimental results. Similarly, two nonphysical model parameters (ERODS and SLIM in LS-DYNA (Ref. 16)), were optimized based on the analyst's past experience and no extensive parameter sensitivity study was reported regarding the influence of physical and nonphysical model parameters on the crush response. Feraboli et al. (Ref. 14), and Wade et al. (Ref. 15) utilized the LS-DYNA progressive failure material model (MAT54) (Ref. 16) to simulate crush experiments of seven different channel and corrugated coupons to further evaluate the suitability of this material model for crush simulation. Results show that MAT54 is capable of reproducing experimental results of different crush geometries, however, two nonphysical parameters, i) the thickness of the crush trigger elements and ii) the MAT54 SOFT parameter (mathematical expedient to avoid global buckling), had to be calibrated for each separate geometry. Although both papers (Refs. 14 and 15) provide the engineering community with additional insight into the influence of parametric variation on the crush response, their FE models cannot be considered a predictive tool.

In this paper, the quasi-static and dynamic crushing response of composite specimens, consisting of a C-channel and a corrugated geometry manufactured with carbon fiber/epoxy matrix fabric, are modeled

using the progressive composite damage model within ABAQUS (Ref. 17). The novel part of this work, which has not been previously addressed in literature, is the associated detailed parameter study conducted to establish the sensitivity of the composite damage model available in ABAQUS with respect to both physical and nonphysical model parameters under a quasi-static crush scenario. The parametric study entails a systematic variation on nonphysical model parameters (contact definition, loading curve, and maximum damage parameter) and physical model parameters (directional strength and fracture toughness) in the C-channel composite panel subjected to quasi-static crushing. C-channel experiments were used to calibrate the model and then refine/optimize a set of material parameters that best fit the experimental results. These identical parameters were then used to simulate the crush response of the corrugated channel specimens, thereby making it a pure prediction and not a double recalibration. Next, the dynamic response of both panels were predicted, further confirming the predictive capability of the developed numerical model. The effect of parameter variation on the crush response is fully documented for future use in engineering applications utilizing this specific ABAQUS damage model. Further geometries are planned to be manufactured and tested in house (under quasi-static and dynamic conditions) to examine the predictive capability of the numerical model in greater detail.

In the next section, details of the specimen design, manufacturing, and testing procedure are described. Next, the constitutive formulation of the built-in composite damage model in ABAQUS are briefly explained. The FE model details, boundary conditions, damage and failure implications in ABAQUS explicit, and model parameters are discussed in a separate section. Comparison of the numerical results with quasi-static and dynamic crush experiments and the parametric study are presented and discussed in detail followed by a conclusion.

Experiment and Specimen Manufacturing

For thin-walled energy-absorbing structures, a typical load-displacement curve during the crushing process is shown in Figure 1. Evaluation indicators are defined to evaluate the crashworthiness of energy-absorbing structures, such as energy absorption (EA), peak crush force (F_{max}), and mean crush force (F_{mean}). The peak crush force (F_{max}) is the threshold value of structural crushing damage to evaluate the difficulty level of the energy absorption of the structure under forcing, which is the initial peak value of the load-displacement curve. The mean crush force (F_{mean}) is the average force of the whole post-peak crushing zone.
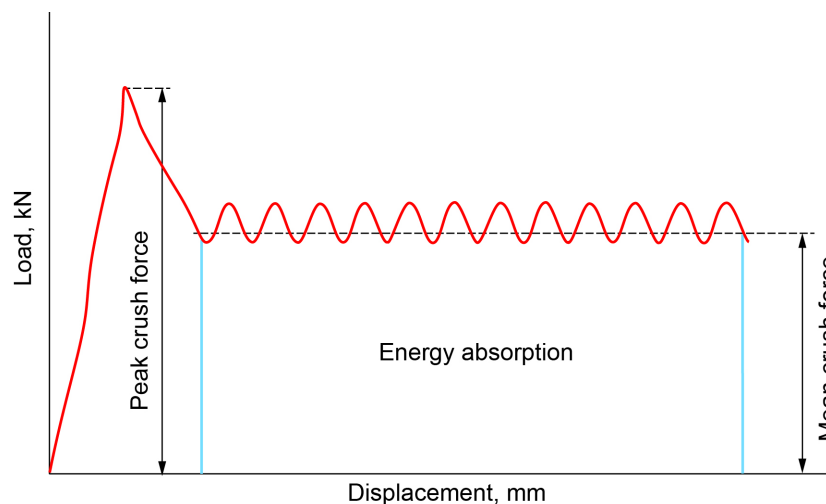

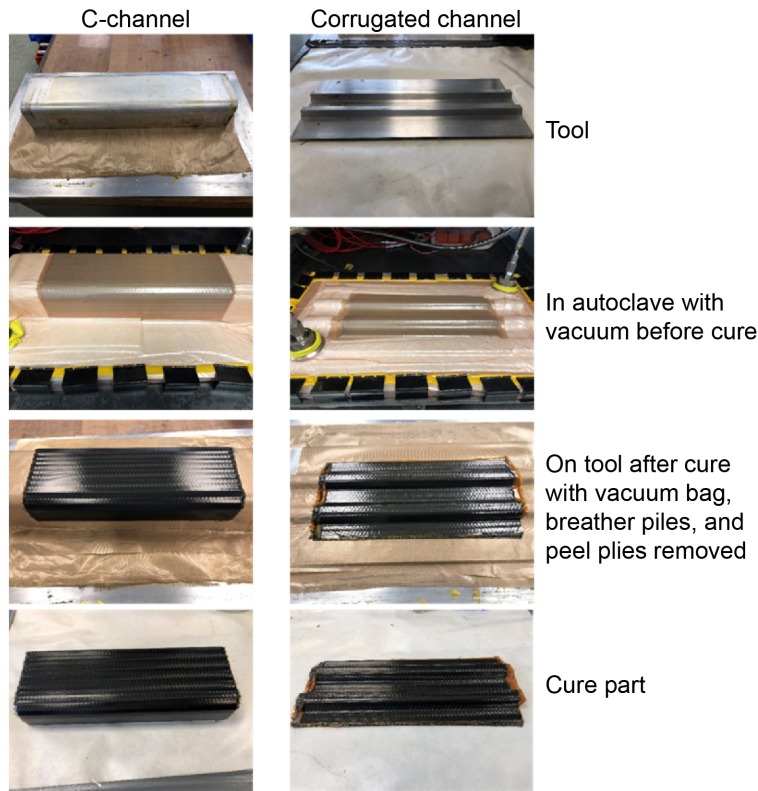Figure 1.—Schematic of typical load displacement with labels defining key terms.

Figure 2.—Processing of composite channel parts.

The material used in this study was a pre-impregnated composite, made from braided T700S carbon fiber and TC275-1 dual-cured toughened epoxy, which had a weight of 536 g (~1.2 lb) and was procured from Tencate Advanced Composites, Morgan Hill, California. The dry carbon fiber braid was manufactured by A&P Technologies, Summerside, Ohio, and consisted of a quasi-isotropic $[0/+60/–60]_s$ braid (QISO H-59) with 24K tows in the axial direction (0° tows) and 12K tows in the bias directions (±60° tows). Test articles were fabricated by hand lay-up of the T700S/TC275-1 on an aluminum tool with the axial tows of each ply parallel to the longitudinal axis of the tool. The laminated part was vacuum bagged and cured, as shown in Figure 2, using an autoclave following the vendor recommended five step cure process: (1) apply full vacuum with an external pressure of 15 psi, (2) heat to 107 °C at a rate of 2.25 °C/min, (3) increase pressure to 85 psi and hold for 60 min, (4) heat to 177 °C at a rate of 2.25 °C/min, (5) release vacuum, hold for 120 min, and cool to 21 °C at a rate of 1.1 °C/min).

Two aluminum tools were used to produce two different composite channel shapes. One type of channel had an open rectangular profile (referred to herein as a C-channel specimen) as shown in Figure 3(a) with different radii defined for the two corners. Another type of channel consisted of a corrugated profile defined in Figure 3(b) (referred to herein as a corrugated specimen). Both channels were made with six composite plies, and the average thickness was 0.135 in. The length of each channel was approximately 14 in., such that two 5 in. long specimens were obtained from each of the produced channels with the profile dimension show in Figure 3.

The specimens were machined with a single-sided 45° chamfer to favor the initiation of stable crushing at one end of the specimen and to avoid undesirable initial spikes in crush loads which may lead to a specimen instability. This chamfer is known as the trigger, or crush initiator. Specimens were then tested in the vertical configuration, resting on a polished hardened steel surface, at a compressive crosshead velocity of ~0.5 in./min. Five repetitions were conducted to obtain average data and ascertain
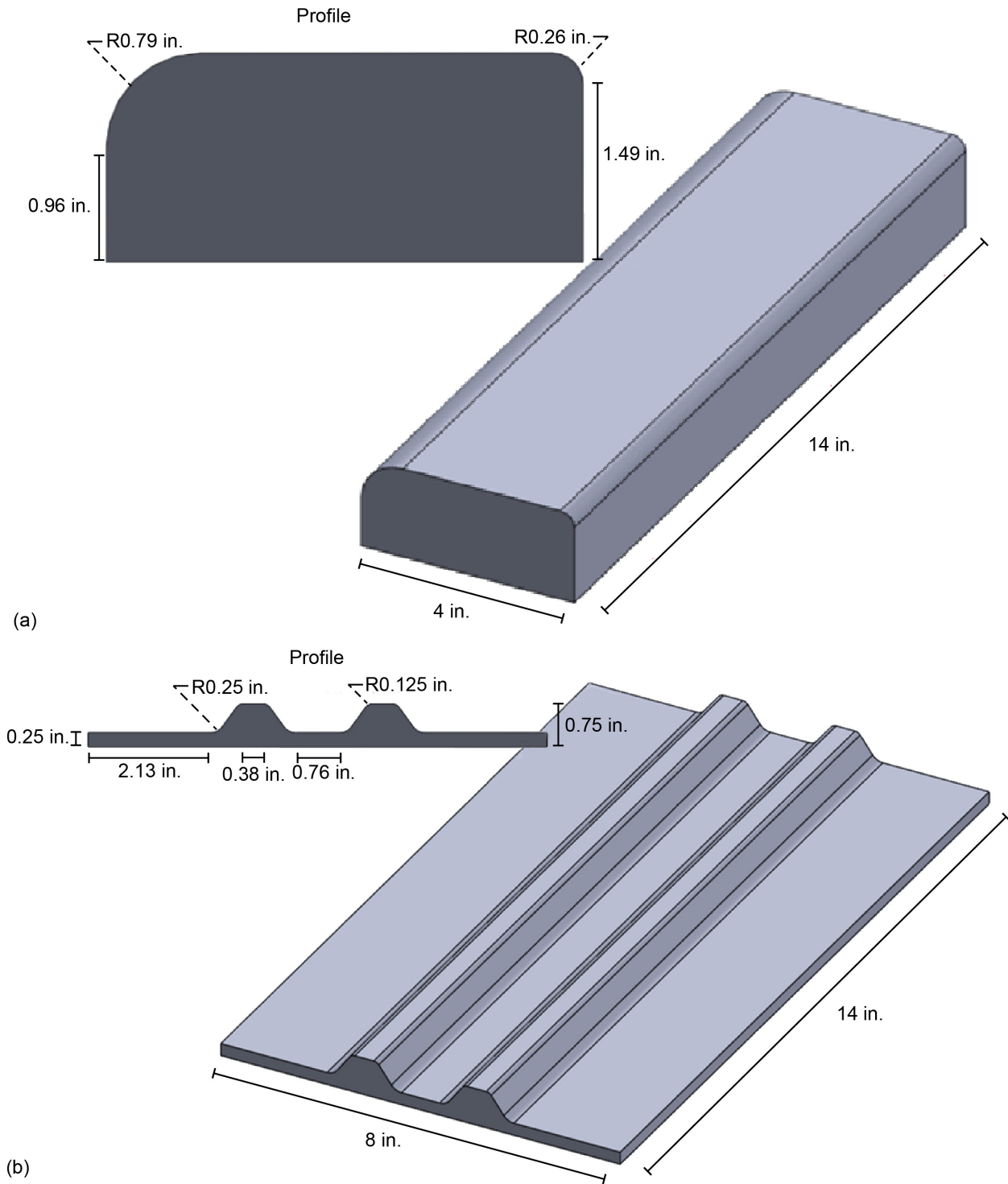
Figure 3.—Molds for different geometries of channel parts (a) C-channel composite mold used to create the C-channel geometry. (b) Corrugated composite channel mold used to create the corrugated geometry.

the repeatability of the experiment. A typical test setup, used for both C-channel and corrugated specimens, is shown in Figure 4(a), and experimental results are summarized in Figure 4(b). As it can be observed from the load-displacement data, good repeatability was achieved for both specimens with a maximum of 11.6 and 3.3 percent variance in average crush load for C-channel and corrugated panels, respectively.
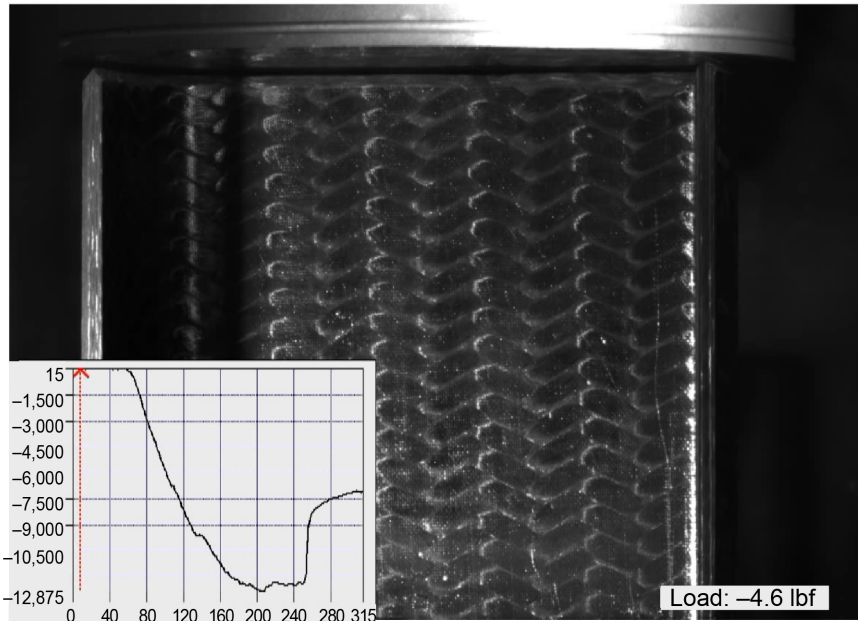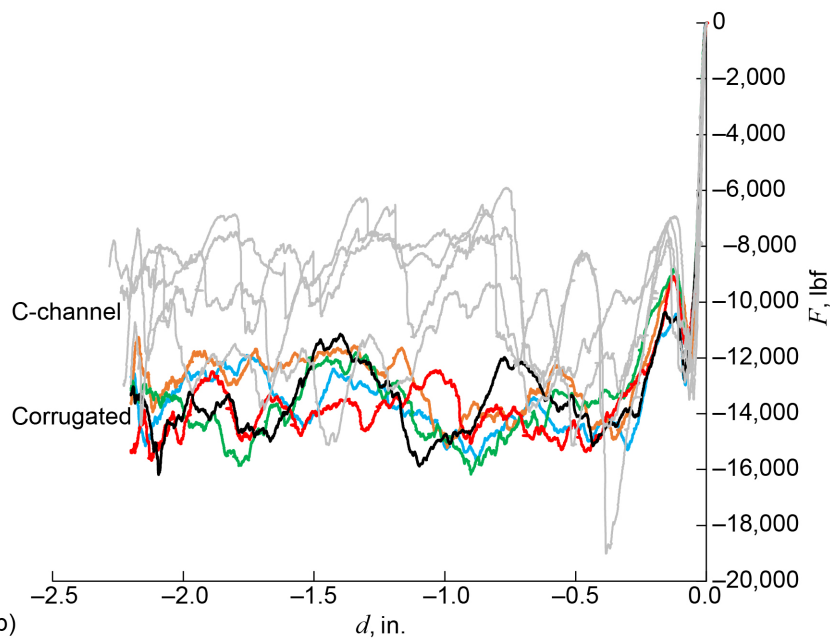
Figure 4.—(a) The crush fixture for C-channel (shown in this picture) and corrugated specimens and (b) summarized load (F)-displacement (d) results for C-channel and corrugated specimens.

"Damage for Fiber Reinforced Composites" Material Model in ABAQUS

The built-in Hashin damage model in ABAQUS (Ref. 17) is used to describe the in-ply damage in each lamina. Each ply is idealized as a transversely isotropic material, with its own five experimentally obtained properties in its undamaged state. Damage initiation, which refers to the onset of degradation of the ply response (Figure 5), is due to four main failure criteria (see Eq. (1)), namely: fiber rupture in
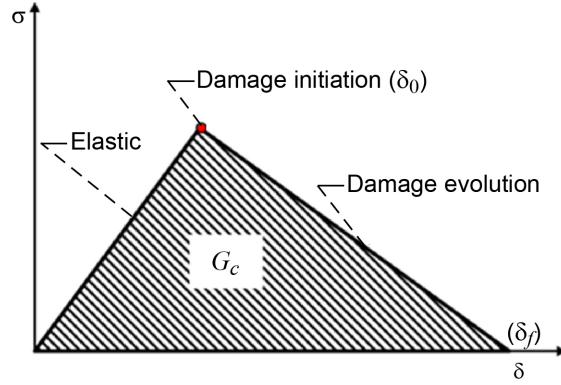
Figure 5.—Stress-displacement behavior with damage
initiation and propagation.

tension (Eq. (1a)), fiber buckling in compression (Eq. (1b)), matrix cracking under transverse tension and shearing (Eq. (1c)), and matrix crushing under transverse compression (Eq. (1d)).

$$\left(\frac{\sigma_{11}^{eff}}{X_t}\right)^2 + \left(\frac{\tau_{12}^{eff}}{S_c}\right)^2 = F_t^f \tag{1a}$$

$$\left(\frac{\sigma_{11}^{eff}}{X_c}\right)^2 = F_c^f \tag{1b}$$

$$\left(\frac{\sigma_{22}^{eff}}{Y_c}\right)^2 + \left(\frac{\tau_{12}^{eff}}{S_c}\right)^2 = F_t^m \tag{1c}$$

$$\left(\frac{\sigma_{22}^{eff}}{S_{tr}}\right)^2 + \left(\left(\frac{Y_c^{eff}}{S_{tr}}\right)-1\right)^2 \frac{\sigma_{22}^{eff}}{Y_c} + \frac{\tau_{12}^{eff}}{S_c} = F_c^m \tag{1d}$$

where X, Y, and S represent the ultimate in-plane strength in the longitudinal, transverse, and shear directions, respectively, and subscripts t and c stand for tension and compression in Equation (1). Since in classical continuum damage mechanics only the undamaged part of a given ply carries the load and transmits stresses, the stresses within the failure criteria should be interpreted as effective stresses, $(\sigma_i^{eff} = \sigma_i / (1-D))_j$. By postulating that the material damage can be characterized mainly by the decrease of load-carrying effective area caused by the development of microscopic cracks, the state of material damage is described by introducing a directional damage parameter D ($D = 1/[1-(1-d_f)(1-d_m)]$ see Eq. (2b)), where d_f and d_m are directional damage parameters in the longitudinal and transverse directions. The relative displacement corresponding to damage initiation (δ_0, Figure 5) for the above-mentioned four various modes depends on the elastic stiffness and the strength parameters specified as part of the damage initiation definition. Once damage initiates, it propagates until the total fracture energy in any of the four mentioned cases reaches its maximum value (G_{cmax}). G_{cmax} corresponds to the area under the triangle in Figure 5, specified by the user for each of the four mentioned damage cases as separate input parameters. During damage evolution, three independent nonnegative in-ply damage parameters, d_f, d_m, and d_s reduce the ply stiffness numerically in the longitudinal, transverse, and shear directions, respectively, until the

final failure point (δ_f, Figure 5) is reached. A mode-specific damage parameter (d) and the degradation of the ply stress tensor (σ) can be written as (Eq. (2))

$$d_{\text{fiber, matrix, shear}} = \frac{\delta_f\left(\delta - \delta_0\right)}{\delta\left(\delta_f - \delta_0\right)}$$ (2a)

$$\sigma = \frac{1}{1-\left(1-d_f\right)\left(1-d_m\right)}\overline{C}\begin{bmatrix}\varepsilon_{11}\\\varepsilon_{22}\\\varepsilon_{12}\end{bmatrix}$$ (2b)

where the stiffness tensor is defined as

$$\overline{C} = \begin{bmatrix} E_{11}\left(1-d_f\right) & \left(1-d_f\right)\left(1-d_m\right)E_{22}\nu_{21} & 0 \\ \left(1-d_f\right)\left(1-d_m\right)E_{11}\nu_{12} & E_{22}\left(1-d_m\right) & 0 \\ 0 & 0 & 1-\left(1-d_f\right)\left(1-d_m\right)\nu_{21}\nu_{12}\left(1-d_s\right)G \end{bmatrix}$$

and E_{11}, E_{22}, and G_{12} are the longitudinal, transverse and in plane shear modulus of the undamaged transversely isotropic lamina, and ν_{12} and ν_{21} are the two Poisson's ratios. Detailed information regarding the mentioned in-ply damage model such as damage evolution laws or constitutive equations can be found in the ABAQUS manual (Ref. 17). Note ABAQUS uses the terminology fiber, matrix and shear even though they speak of lamina properties, that is they associate the fiber with the longitudinal direction, the matrix with the transverse, and shear with the in-plane shear components.

Description of the FE model

The geometry of both C-shaped and corrugated panels consists of fabric plies meshed with quadrilateral continuum shell elements (SC8R) with 3 translational degrees of freedom, utilizing homogenized "composite-layup" in ABAQUS. The model was kept as homogenized to make comparisons with the available results obtained through LS-DYNA in a previous internal study. Using shell elements is a better option compared to 3D solid elements for capturing out-of-plane plate bending. As a result of a mesh study (see results section for details) a uniform square element mesh density with element size of 0.04 by 0.04 in. was used to optimize efficiency and also avoid aspect ratio problems in highly distorted elements for both geometries. The total number of elements employed for the C-channel and corrugated panel were 132,774, and 120,328, respectively. The in-plane response of the fabric plies was simulated with the built-in constitutive damage model in ABAQUS described in Equation (1). All input material parameters (see Table I) for the composite layup were obtained from previous available in-house quasi-static experimental measurements. Required model parameters are:

a) Elastic properties (longitudinal, transverse, and in-plane shear modulus) under tension and compression,
b) Ultimate in-plane strength under tension and compression in the longitudinal, transverse and shear directions, respectively
c) Laminar fiber fracture and matrix cracking energies.

TABLE I.—BASELINE ROOM-TEMPERATURE LAMINA PROPERTIES

Model parameter	Tension	Compression
Longitudinal Young's modulus, E_{11}, Msi	6.55	6.26
Transverse Young's modulus , E_{22}, Msi	6.34	6.06
Longitudinal Poisson's ratio, ν_{12}	0.24	0.24
Longitudinal shear modulus, G_{12} , Msi	2.38	2.38
Transverse Poisson's ratio, ν_{21}	0.21	0.21
Longitudinal strength, X, ksi	134.9	82.5
Transverse strength, Y, ksi	127.7	61.4
Shear strength, S_L, ksi	34.3	34.3
Transverse fracture toughness , in.*lb/in.^{2}	3.1	3.1
Axial fracture toughness, in.*lb/in.^{2}	20	20

The compressive crushing load was applied to the composite plate through another solid rigid plate (Rigid Body) moving with a constant velocity of (900 in./min). The smooth step definition method in ABAQUS was utilized to define applied loading and avoid sudden changes in load application. This method can be used to define the amplitude (loading) between two consecutive data points to ramp up or down smoothly from one amplitude value to another. As with any other explicit solver, to achieve efficient and economic quasi-static simulations, either the loading rate has to be artificially increased, or mass-scaling (artificially increasing the material density) should be utilized. In order to make sure the increase in the rate or the mass did not influence the solution, the kinetic energy (KE) of the plate was checked and compared to the internal energy of the system. As long as the KE was a small fraction of the internal energy (KE < 1 percent of internal energy), inertial effects were considered to be negligible. Here, this artificial increase of the loading velocity has no effect on the analysis results; dynamic effects only become significant beyond a velocity of (3000 in./min). For dynamic simulations, the velocity is set to be 52800 in/min (50 mph) as tested at the GRC dynamic impact Lab. At these high velocities inertia effects become significant, and the mass/inertia matrix should be constituted carefully. No mass scaling was used in this analysis. The thickness of one layer of elements in the top portion of the specimen was halved to simulate the 45° chamfer acting as a crush initiator/trigger. In other words, the trigger is modeled as a single row of reduced thickness elements at the crush front of the specimen. The contact between the composite and the test rig were modeled using both the general contact and contact pair algorithms of ABAQUS explicit (see next section for comparison). After damage initiation and final propagation, the general contact definition was automatically updated to account for possible post-damage contact. A snapshot of the FE model for both geometries are shown in Figure 6 with fixed base support (modeled as a rigid body), and without base support (with fixed boundary conditions at the bottom of the composite plate to save computational time). These two boundary conditions (with and without base support) were studied further to see if removing the bottom rigid support and eliminating boundary nonlinearity (contact) could further improve model efficiency without compromising accuracy (more detailed results are reported in the next section).

Results and Discussion

Initially, a preliminary mesh study was conducted to determine an adequate mesh density optimizing both calculation efficiency and accuracy. The C-channel specimen was meshed uniformly using four

different square element sizes (0.01, 0.02, 0.04, and 0.08 in.) with the exact same meshing algorithm (medial-axis). The medial axis algorithm in ABAQUS first decomposes the region to be meshed into a group of simpler regions. The algorithm then uses structured meshing techniques to fill each simple region with elements. This algorithm is faster in generating a quadrilateral and hexahedral mesh (in our specimens) for noncomplicated geometries. Results are shown in Figure 7(a). The analysis with the 0.08 by 0.08 in. in element size ended prematurely due to excessive mesh distortion, rendering this low density mesh useless for our crushing analysis. The load/displacement response of the 0.02 by 0.02 in. and the 0.04 by 0.04 in. mesh were almost identical, with the latter being four times more efficient computationally. The load-displacement response for the most dense and computationally expensive mesh size (0.01 by 0.01 in.) was very similar to the above-mentioned meshes with slight differences in the mean crushing load section. Considering the results shown in Figure 7(a), for a composite plate with similar dimensions and geometry, it is recommended that a 0.04 in. square element mesh size be used; as this maintains a balance between solution accuracy and efficiency. Given the highly nonlinear nature of the crushing scenario, any model adjustment that can improve computational time without compromising accuracy is of great value. Accordingly, the base support was also removed here, and the bottom of the plate was fixed in place, to check for any variations in the load/displacement response. With a minimal difference observed in load/displacement results (Figure 7(b)), fixed boundary conditions can be applied to the bottom of the specimen eliminating the need to model the base support and thus, saving significant computational time.
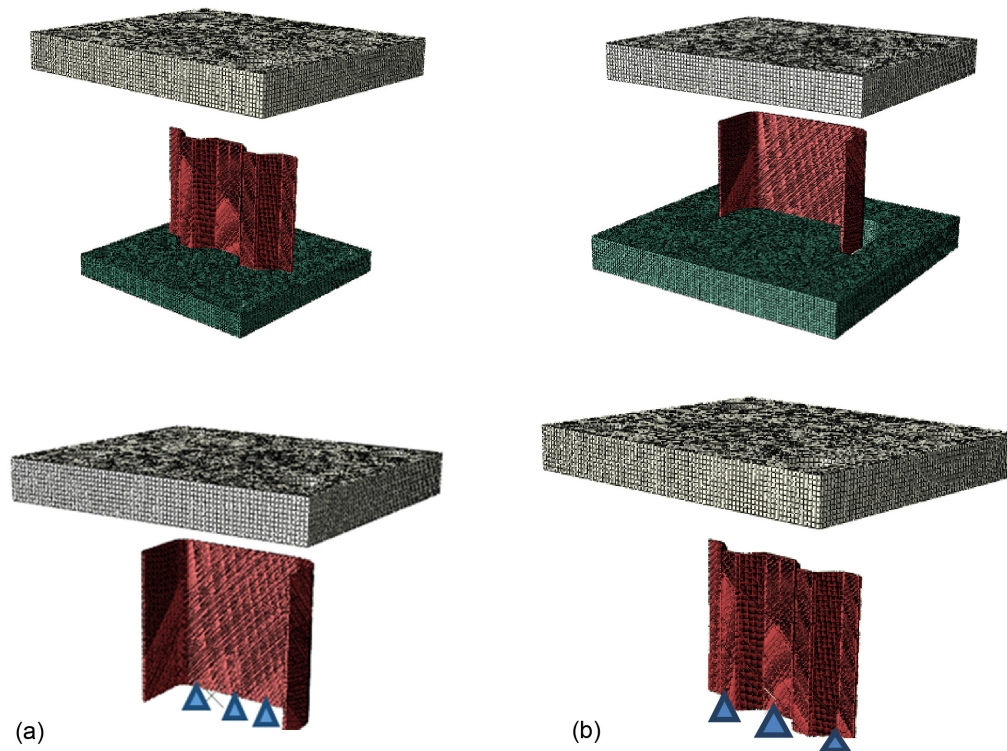

Figure 6.—A snapshot of the FE model for both C-channel (a) and corrugated (b) geometries with and without base support (with fixed boundary conditions at the bottom of the plate).
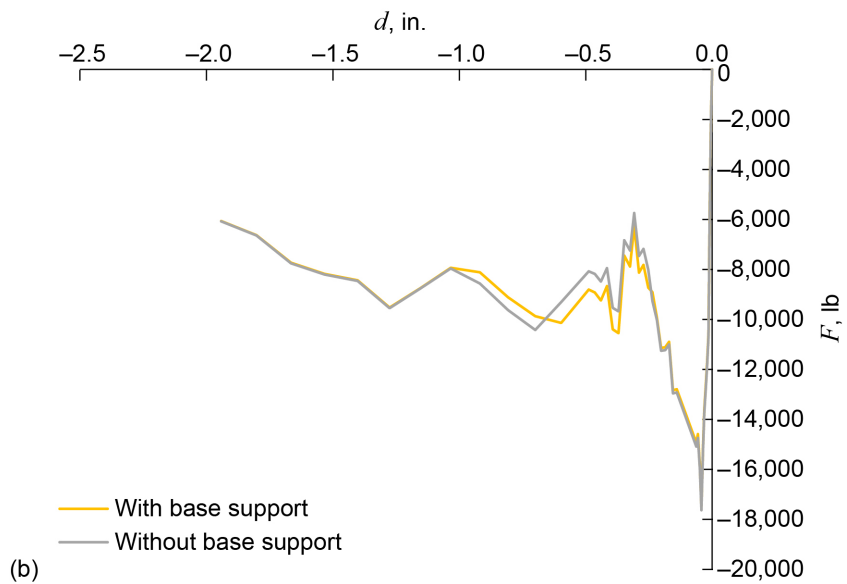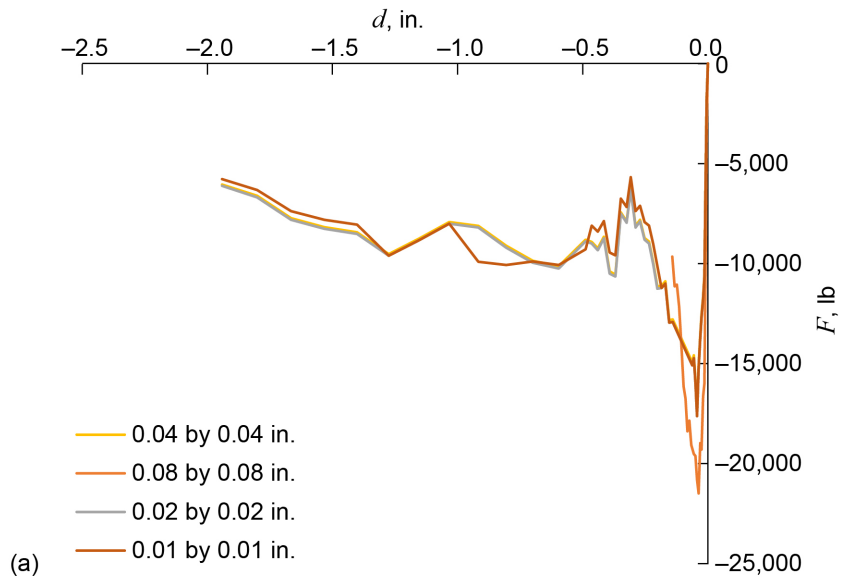
Figure 7.—(a) Load (*F*)-displacement (*d*) results for C-channel with varying mesh size. (b) Load-displacement results for C-channel with and without base support.

After studying mesh quality and improving computational efficiency, a variation of 10 to 20 percent was applied to strength and fracture toughness parameters to investigate the sensitivity of material variations on the load-displacement response of the C-channel composite panel. In addition to experimentally measurable material properties, the effect of nonphysical model parameters (contact definition, loading curve, and maximum damage parameter) on the crushing response of this panel was also studied and reported in the next section. After developing an optimized set of physical and nonphysical model parameters for the C-channel composite panel, identical model parameters were used to *predict* the crushing response of the corrugated panel subjected to the same loading scenario.

Parametric Study—C-Channel

First, physical model parameters (strength and fracture toughness) were varied 10 to 20 percent from baseline values (measured in-house experimentally, Table I) to observe the effects on the crushing response. Next, nonphysical model parameters were varied to further improve the results. After studying the influence of physical and nonphysical model parameters on the load-displacement response of the C-channel, an optimized set of model parameters was utilized to make the final comparison with the experiments.

Effect of Strength

Experimentally measured directional strength values were varied simultaneously between 10 to 20 percent to assess the effect of these changes on the load-displacement response of the C-channel panel. As observed from Figure 8, a homogenous decrease/increase of 10, 15, and 20 percent in the compressive and shear strengths has a notable impact on the peak load, and implicitly affects the post-peak part of the crushing response. The pre-peak slope is primarily dominated by elastic moduli. The elastic moduli values used in the simulations reproduce the pre-peak slope of the crushing response, and hence, there is no need for a parameter study including elastic moduli variation. Variations in tensile directional strengths demonstrated negligible effects on the load-displacement response, and therefore, the results are not included in Figure 8. The yellow curve (baseline strengths) shows the load-displacement response with experimentally measured strength values. Considering experimental variability, one can argue that the baseline curve is a reasonably good simulation of the crushing scenario, with the difference being within experimental scatter. However, the major point of this study is not only matching the experiments, but also learning how parameter variation affects the crushing response. With a 15 percent decrease in the directional (transverse) compressive and shear strength, a better match with the experiment (averaged curve included in the figure) was obtained, where the peak load was captured with less than 3 percent error. It is observed that increasing the initiation strength causes a sharp drop in the post-peak section leading to a lower mean crush load. This is probably due to all elements failing simultaneously after most of the energy is consumed to initiate failure. Whereas, lowering the initiation strength seems to instigate higher mean crush loads (post-peak) where more energy is dissipated out of the composite specimen during the propagation phase. This suggests that a composite system with a lower initial strength might be better than a high-strength layup in absorbing crush energy (i.e., high volume fraction of [0] layers in the loading direction might not be a desirable design idea for increasing energy absorption in a crush scenario). This can be investigated further using micromechanics. Also note that the decrease/increase in the peak load is not linearly correlated with the decrease/increase in the directional strengths, which is to be expected in a nonlinear crush scenario.
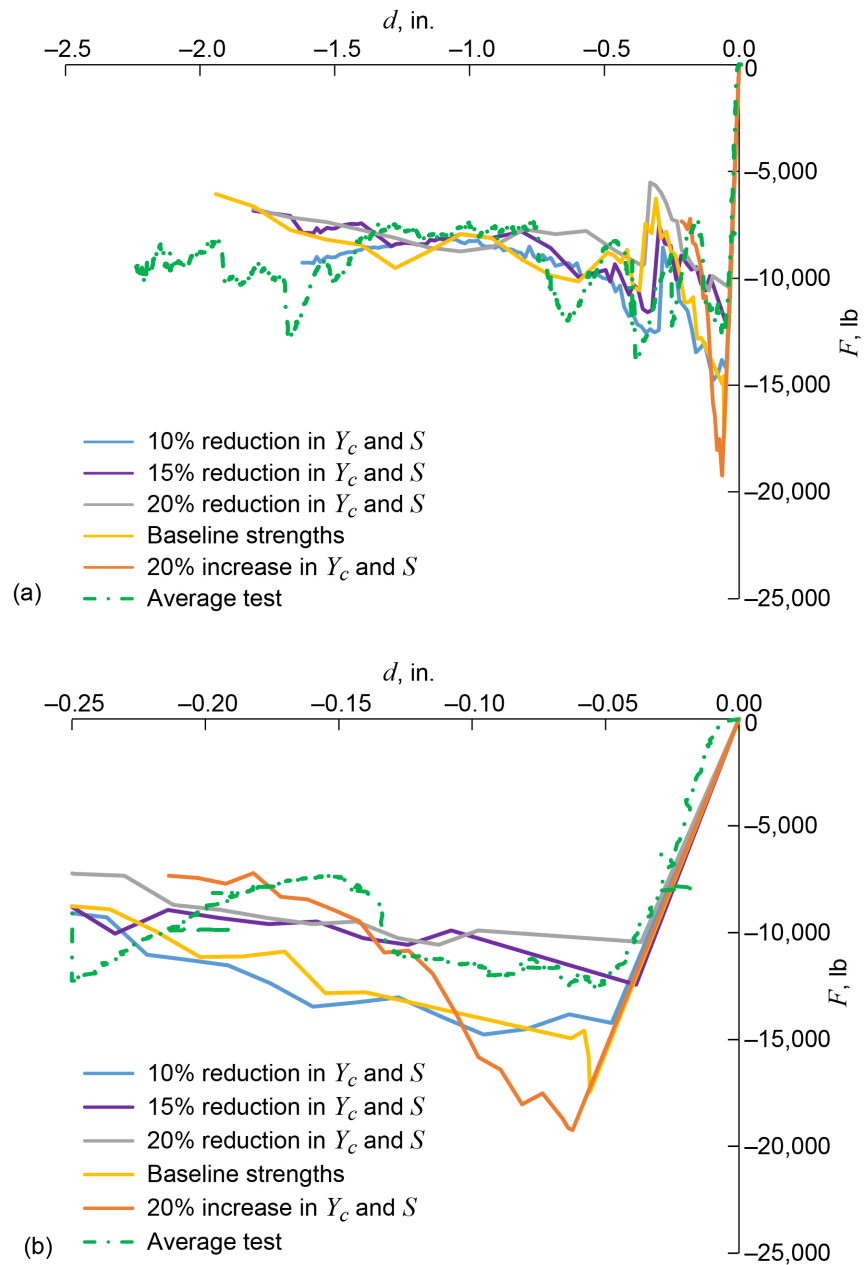
Figure 8.—Influence of initiation failure strengths on the load-displacement response of C-channel geometry: (a) complete load-displacement response, (b) initial load-displacement response curve enlarged to better visualize the pre-peak region.
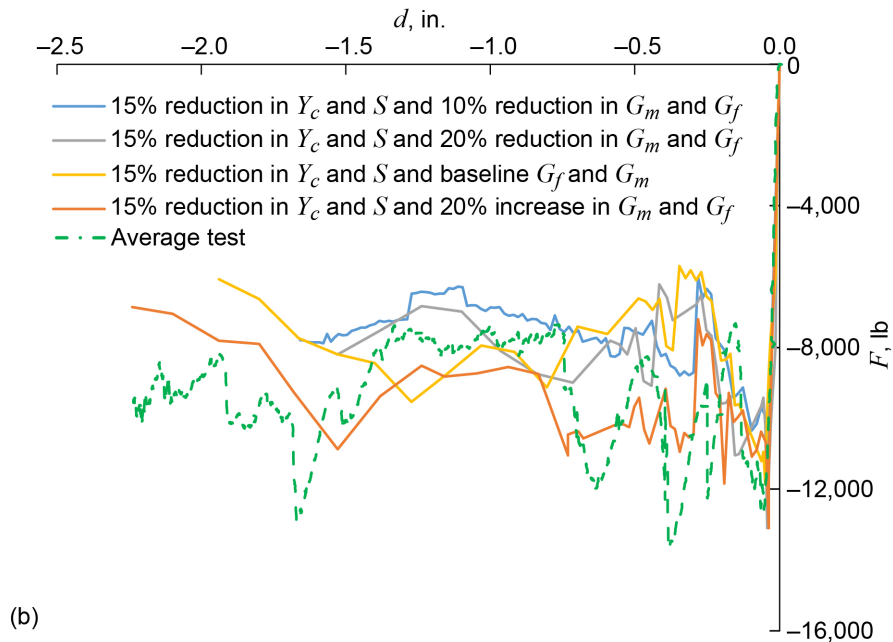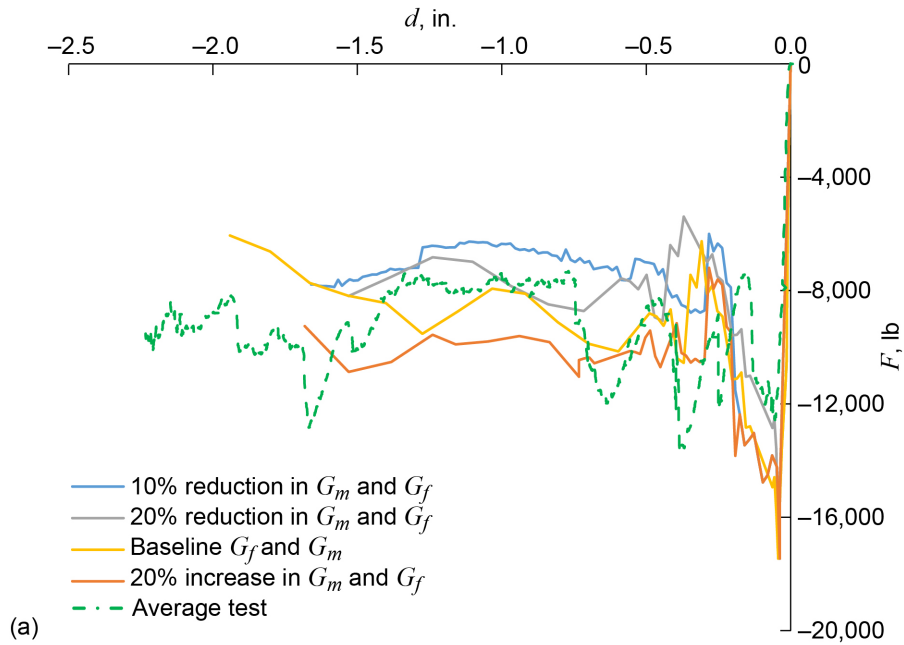
Figure 9.—(a) Influence of fracture toughness parameters on the load-displacement response of C-channel geometry. (b) Combined influence of fracture toughness parameters on the load-displacement response of C-channel geometry with a 15 percent reduction in transverse compressive and shear strength.

Effect of Fracture Toughness

The quasi-static crush response of the C-channel is examined in this section with respect to variations in fracture toughness values. As illustrated in Figure 9, a 10 to 20 percent decrease/increase in directional fracture toughness affected the post-peak mean crushing load of the composite panel, while the peak load itself remained unchanged. With higher/lower fracture toughness values, the mean post-peak crush load seems to be higher/lower, respectively. The yellow curve (baseline fracture toughness) shows the load-displacement response given experimentally measured parameter values. Although some influence on the post-peak mean crush load was observed with varying fracture toughness, all the curves in Figure 9 fall within an acceptable experimental margin. It is also worth mentioning that there is no set standard for measuring in-plane fracture toughness in a composite panel, much less a braided composite. Although there have been widely used tests such as compact tension, double cantilever beam or notch fracture in the literature (Refs. 18 and 19). A wide variability in the in-plane fracture toughness values due to the testing method is common. This can make the variation margin much larger for the purpose of a parametric study, which might in turn have significant effects on the post-peak mean crushing load of a composite panel. However, since a change of 10 to 20 percent from the experimental fracture toughness values measured at GRC yields reasonably good results, no further variations have been studied here.

Figure 9(b) illustrates the combined effect of changing the compressive and shear directional strengths together with fracture toughness. With the experimental variability observed in a given crushing scenario, picking a load-displacement curve closest to the average experimental data is very subjective. Here, a combination of a 15 percent reduction in strength and a 20 percent increase in fracture toughness seems to capture the peak load, the post-peak crush regimen and the final displacement very closely. Due to this increase in facture toughness (larger area under the triangle in Figure 5), the post-peak crushing seems to have a longer progression, leading to a higher final displacement compared to other curves.

Effect of Maximum Damage Parameter

As described previously in the material model description section, the directional damage parameters d_f, d_m, and d_s reduce the respective ply stiffness (through the stiffness tensor of the material point, $\bar{C}$) numerically in the longitudinal (fiber), transverse (matrix), and shear directions for any given element until the final failure point is reached. In ABAQUS explicit, the user has control over how elements with severe damage are treated. By default, the upper bound to all damage variables at a material point is $d_{max} = 1$. However, the user can reduce this upper bound to stabilize the failure. A material point is assumed to fail when either of the damage variables associated with fiber failure modes (tensile or compressive) reaches the assigned maximum d_{max} value. The element is removed from the mesh when this condition is satisfied at all of the section points at any one integration location of an element. For example, in the case of shell elements (used in this analysis) all through-the-thickness section points (top/middle/bottom location of a given ply) at any one integration location of the element must fail before the element is removed from the mesh. If an element is removed, it offers no resistance to subsequent deformation. Alternatively, the user can specify that an element should remain in the model even after all of the damage variables reach the assigned d_{max} value. In this case, once all the damage variables reach the maximum value, $\bar{C}$ remains constant (see the expression for $\bar{C}$ in the previous section). Here the element deletion option is turned off due to convergence issues in ABAQUS explicit. As one can see from Figure 10, the analysis could not be completed with the default high value of d_{max} (0.99). For example, all the section points along composite thickness could reach the defined maximum d_{max} value, except one, which did not reach the specified value even after increasing the number of iterations in a given
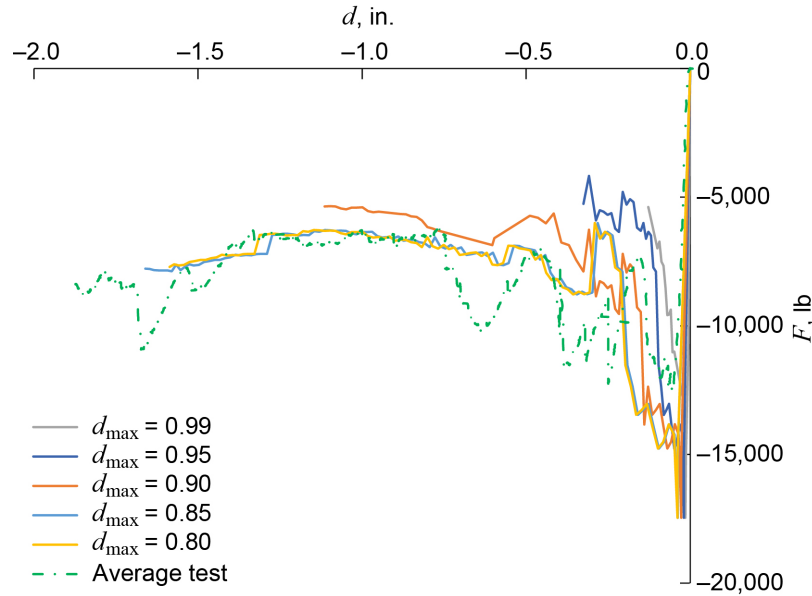
Figure 10.—Influence of maximum damage parameter on the load-displacement response of C-channel geometry.

increment. This made the analysis unstable and the convergence unlikely, leading to premature end of analysis. Although a completely damaged element is typically defined as an element with a $d_{max} \sim 1$, one can still lower the limit to a reasonable degree and achieve similar results. In order to mitigate the instability caused by the default d_{max} definition in ABAQUS and also to understand the influence of d_{max} on load-displacement response, this variable was varied between 0.81 to 0.99 in the analysis and the results are summarized in Figure 10. As observed in Figure 10, the results for $d_{max} = 0.90$, $d_{max} = 0.85$, and $d_{max} = 0.81$ match the experiment within an acceptable margin, and the analysis instability is resolved by assigning $d_{max} < 0.9$. Decreasing d_{max} beyond 0.81 was not deemed as a suitable definition for a maximum value of a damage parameter, and therefore no further reductions in d_{max} were studied. One can see that the change in d_{max} affects the post-peak slope of the load-displacement curve, but not the peak load itself. This, in conjunction with some variation in fracture toughness values, can be utilized as a very useful tool to gain more control over the post-peak slope in a crush scenario while preserving the peak load, as long as d_{max} is only lowered to a reasonable value, i.e., $d_{max} > 0.8$.

Effect of Loading Curve

ABAQUS has a simple, built-in smooth step amplitude curve that automatically creates a smooth loading amplitude. One can apply a displacement/velocity with a smooth step amplitude curve using only the initial and final data points, and the intervening motion will be smooth. A small scale study was performed on the slope of the smoothing curve (by shifting the data points) to see how it might influence the load-displacement response of the C-channel subjected to crush loading. It was observed that as long as the initial applied velocity does not approach dynamic limits, various smoothing curve slopes have a very negligible effect on the pre-peak and post-peak portions of the load-displacement response.

Effect of Contact Definition

Contact is an extremely discontinuous form of nonlinearity. ABAQUS explicit provides two algorithms for modeling contact; general contact and contact pairs. In the general contact algorithm all bodies in the model are included with default surfaces being defined automatically, however, the user is allowed to include/exclude more surface pairs. For the contact pairs algorithm, interactions must be defined manually by specifying each of the individual surface pairs that can interact with each other. The contact constraint is the penalty method for general contact algorithm, and kinematic compliance method for the contact pairs. In most cases the kinematic and penalty algorithms will produce nearly the same result, therefore, no parametric study was done here on the constraint method. Detailed information about contact algorithms and contact constraints can be found in the ABAQUS manual (Ref. 17). Although the general contact algorithm is considered to be generally faster for large models, manual definition of contact surfaces in a crash scenario can reduce the simulation time to a great extent. Additionally, contact pairs algorithm allows for the contact surfaces to be activated and deactivated throughout the analysis history to optimize the speed. These two contact definitions were utilized between the impactor and the specimen to assess the influence of the contact algorithm on simulation speed and convergence. Contact was defined utilizing the commonly used node-to-surface feature for both algorithms. Impactor and specimen faces were chosen manually for the contact pair algorithm to minimize unnecessary contact solutions. As it can be seen in Figure 11, both methods yield a similar load-displacement response with the contact pair algorithm being marginally faster than the general contact algorithm (390 vs. 415 min), with more noise. Considering all the manual effort that has to be done to optimize the contact pair algorithm, a general contact algorithm is a much more efficient option to be used with three-dimensional crush scenarios. It is also worth mentioning that there was no interpenetration between contact faces up until the very last stages of crushing where the plate had fully failed, and the small sliding energy was negligible.
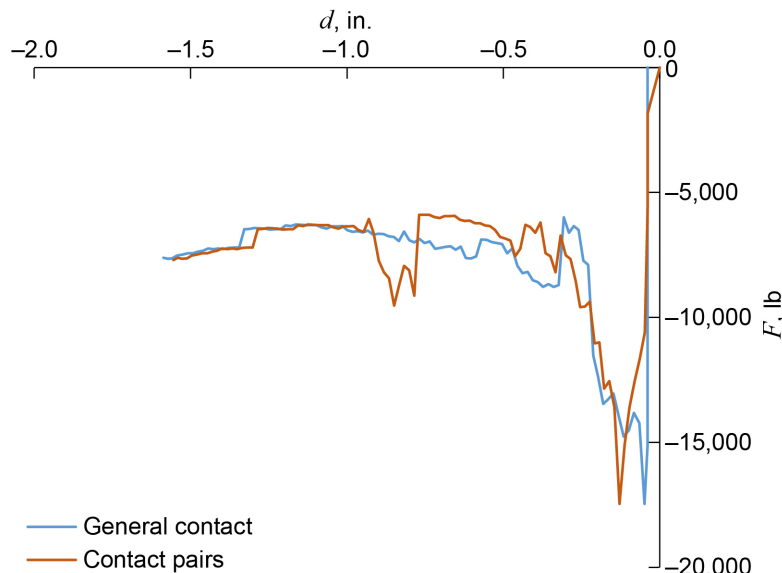

Figure 11.—Influence of contact definition on the load-displacement response of C-channel geometry.

Panel Simulations (Quasi-Static)

C-Channel

After studying the influence of physical and nonphysical model parameters on the load-displacement response of the C-channel, an optimized set of model parameters (Table II) was compiled to model the crushing response of this panel and compare it to experimental results (Figure 12). This was done by picking the properties that provide the best (subjective) fit with the experimental results. As mentioned earlier, one can say that the baseline curve provides a reasonably good simulation of the crushing scenario, considering experimental variability. However, this study aims to shed more light on how

TABLE II.—OPTIMIZED/IMPROVED MODEL PARAMETERS
(BOLD SHOWS THE VALUE FOR DYNAMIC SIMULATIONS)

| Model parameter	Tension	Compression
Longitudinal Young's modulus, E_{11}, Msi	6.55 (**9.5**)	6.26 (**9.5**)
Transverse Young's modulus , E_{22}, Msi	6.34 (**9.5**)	6.06 (**9.5**)
Longitudinal Poisson's ratio, v_{12}	0.24	0.24
Longitudinal shear modulus, G_{12}, Msi	2.38	2.38
Transverse Poisson's ratio, v_{21}	0.21	0.21
Longitudinal strength, X, ksi	134.9	82.5
Transverse strength, Y, ksi	127.7	52
Shear strength, S_L, ksi	34.3	27
Transverse fracture toughness, in.*lb/in.^{2}	3.8	3.8
Axial fracture toughness, in.*lb/in.^{2}	24	24
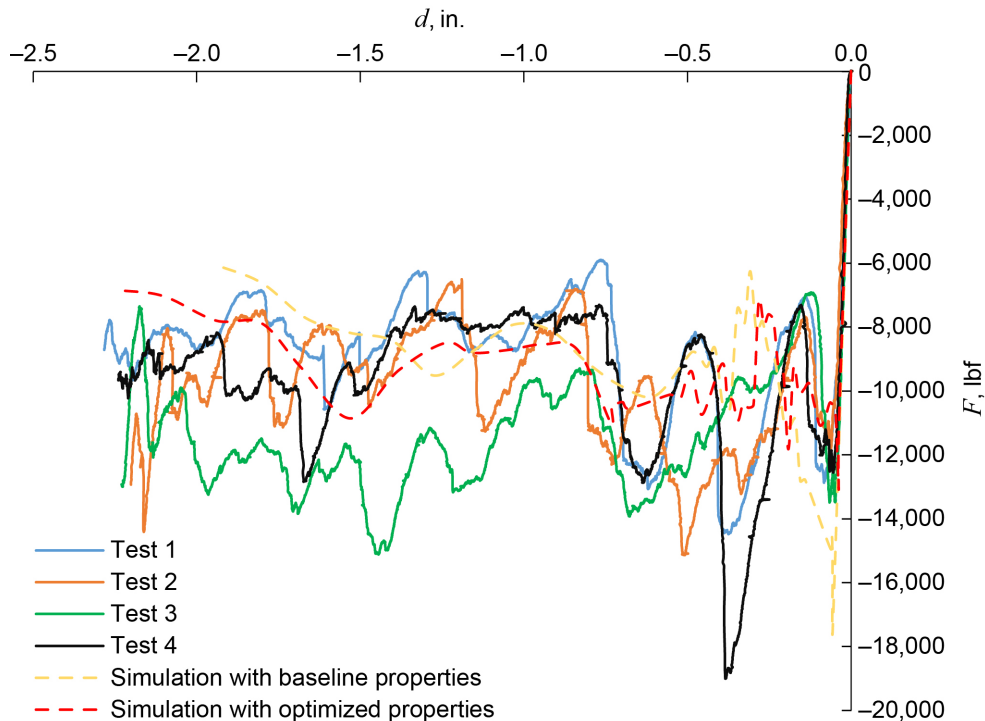
Figure 12.—Load (F)-displacement (d) response of the C-channel compared with experiments.
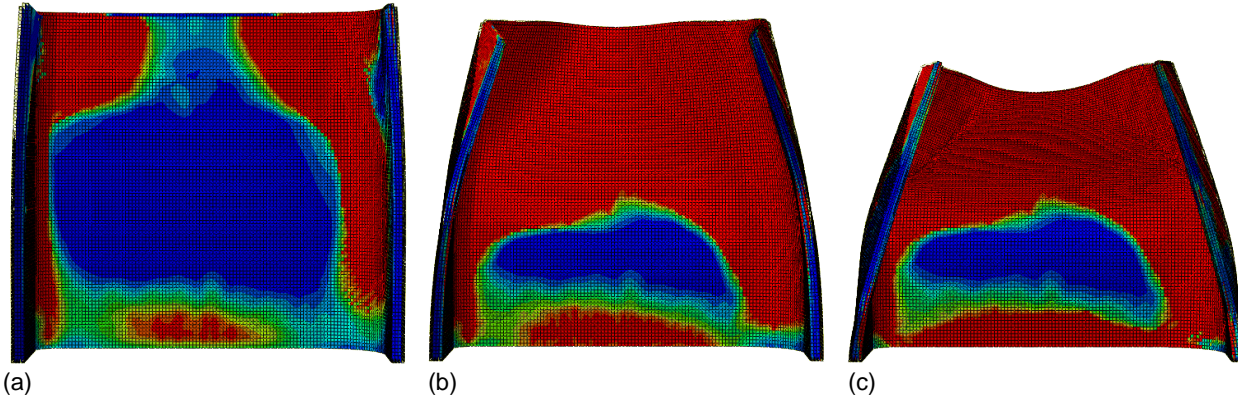
Figure 13.—Failure pattern of the C-channel (red elements are progressively failed elements—snapshots taken at (a) peak load, (b) 1 in., and (c) 2 in. displacement points).

parameter variation affects the crushing response rather than just matching the experiments. Modified physical parameters from baseline (see Table I) are shown in red in Table II. One can see that a better agreement was observed between numerical and experimental results (especially in peak load and failure displacement estimations) without significant deviation from experimentally measured physical model parameters. The most dominant failure criterion is matrix crushing under transverse compression (criterion 1d, Eq. (1)) for damage initiation. In the post-peak region, damage caused by fiber compression (criterion 1b) also plays an important role during propagation and element failure. Figure 13 illustrates the progressive failure pattern of the panel with an initial O-shaped fracture of the web followed by folding failure. It is obvious that most of the crushing damage occurs between peak (Figure 13(a)) and 1 in. (Figure 13(b)) displacement points, where a large number of elements fail. A similar failure pattern was captured in a video by the experimental team. It is worth mentioning that there was some visible delamination in the video past the 1.3 in. displacement point preceded by transverse matrix crushing and fiber compression, which are the main failure mechanisms for this panel. Because some visible delamination was observed in later phases of the crushing, this model captures the major failure pattern correctly up to the delamination initiation point. This is of significant value, as any load-displacement response can be matched with experiments without capturing delamination. Although including delamination in the model is an ideal approach to fully capture the failure process, it would greatly reduce the computational efficiency of the model. Considering the fact that this study is geared towards the engineering community, computational efficiency of the model is of great value; consequently the benefits and drawbacks of adding delamination to the model should be weighed carefully before including it in the model.

Corrugated Panel

The optimized set of physical and nonphysical model parameters (Table II) achieved through the parametric study for the C-channel were used to predict the crushing response of the corrugated panel subjected to the same loading scenario. Because, identical parameters were used to reproduce the crush response of this panel, the results are considered *pure predictions* and not a recalibration. As it can be seen from Figure 14, the model is in very good agreement with experimental results and it can be reliably used to do further predictions for this material system providing the failure mechanisms do not change. The effect of optimizing model parameters is more evident for this panel. The peak load, post-peak part of the load-displacement curve, and the final failure displacement are definitely in better agreement (red

dashed line) with experimental results compared to the simulation conducted with baseline properties (yellow dashed curve). The more notable effect of varying properties on this geometry might be due to its more complicated shape creating a more torturous path for the damage progression. The damage progresses in a smoother/ more progressive manner, and therefore, the experiments are more repeatable (as seen from the tests in Figure 14), eliminating extreme fluctuations. Moreover, the crushing behavior of the geometry becomes more sensitive to parametric variation. The failure pattern of the corrugated panel is depicted in Figure 15, where one can see initial fracturing of the top portion followed by corner fractures spreading along the entire specimen. Similar findings were observed in the video captured in the GRC impact lab. Similar to the C-channel there is some visible delamination in the video in later phases of the crushing so the model can be said to capture the major failure pattern correctly up to the delamination initiation point.
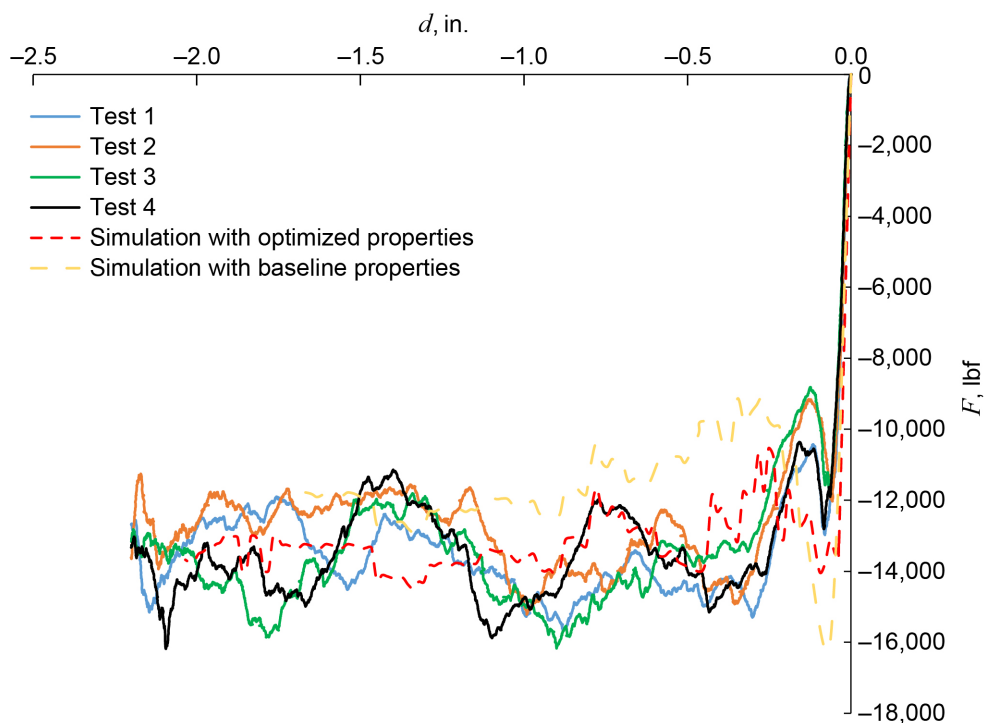

Figure 14.—Load (F)-displacement (d) response of the corrugated panel compared with experiments.
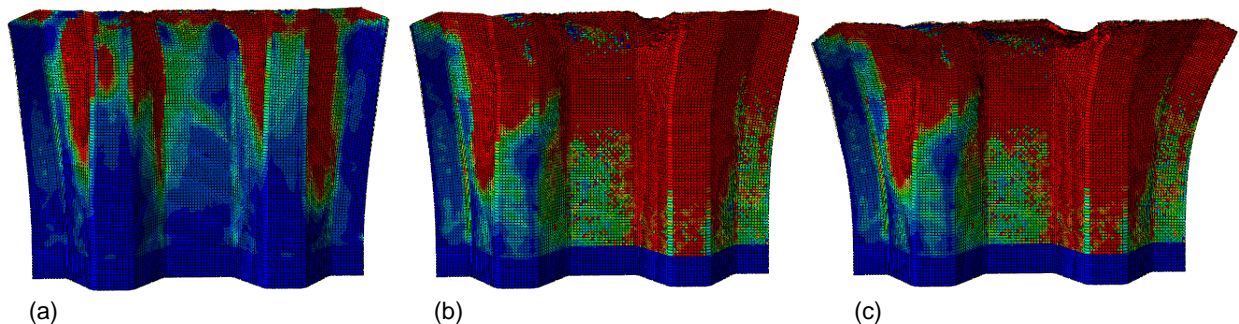

(a) (b) (c)

Figure 15.—Failure pattern of the corrugated panel (red elements are progressively failed elements—snapshots taken at (a) peak load, (b) 1 in., and (c) 2 in. displacement points).

Panel Simulations (Dynamic)

C-Channel and Corrugated Panel

After successfully modeling the quasi-static response of both the C-channel and the corrugated panel, the dynamic response of both plate specimens were predicted using the same optimized set of model parameters (Table II). Only the elastic moduli was adjusted manually to account for known rate dependent (dynamic) effects (adjustments are highlighted in blue in Table II). Note for better accuracy one should use a truly rate-dependent, large strain, constitutive model (e.g., viscoelastoplastic); however once again this would significantly add to the computational expense. In Figure 16, the dynamic load-displacement response of the C-channel subjected to 52,800 in./min (50 mph) impact is compared with the corresponding experiment conducted by the GRC impact lab. The numerical load-displacement curve matches the experimental data (a representative average of 3 dynamic tests) relatively well considering the highly non-linear nature of a dynamic crush scenario. Meanwhile, Figure 17 demonstrates the dynamic failure pattern of the C-channel with an initial centered fracture followed by a rapid break along both corner lines. Next, Figure 18 shows the comparison between the dynamic load-displacement response of the corrugated panel subjected to 52,800 in./min (50 mph) impact with the corresponding experiment. A relatively good match is achieved for this specimen as well, with the specimen undergoing severe matrix crushing/fragmentation of the top portion (Figure 19) followed by a rapid growth throughout the whole specimen.
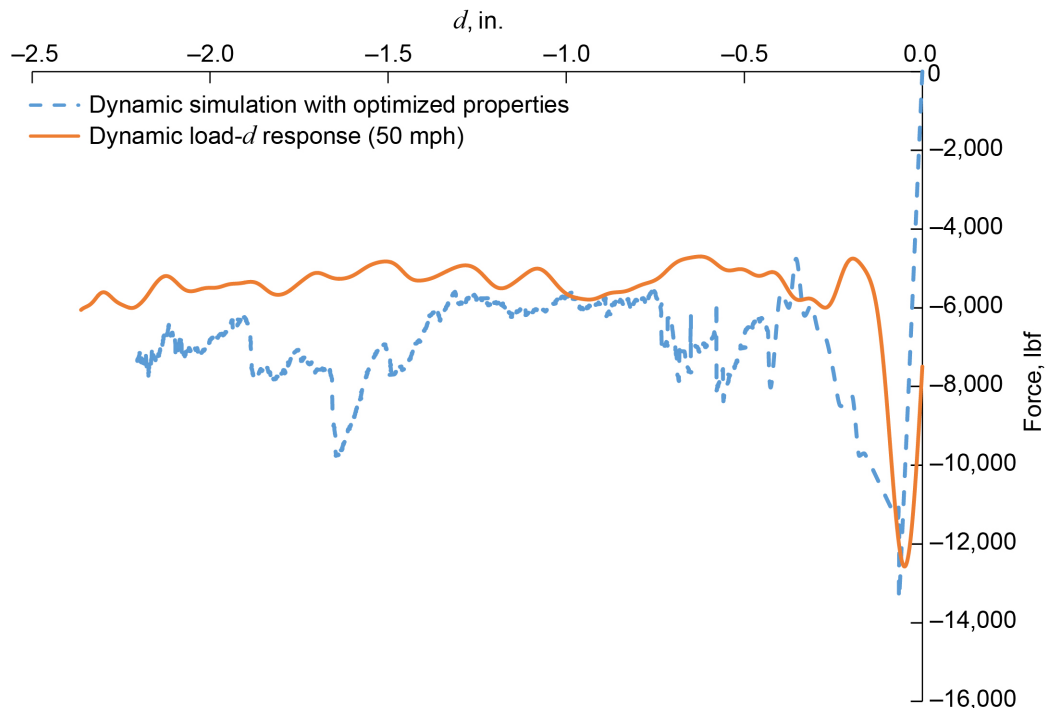

Figure 16.—Dynamic load-displacement (d) response of the C-channel compared with experiments.
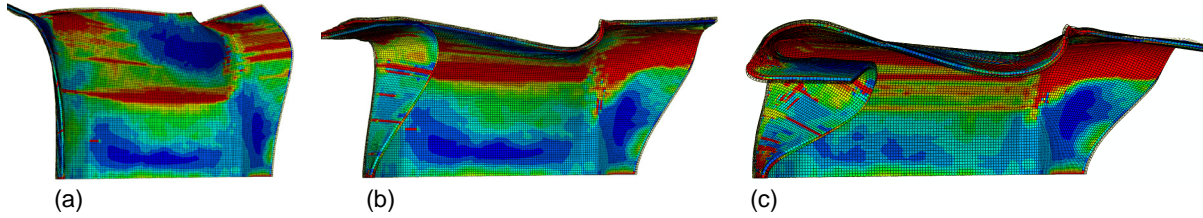
Figure 17.—Failure pattern of the C-channel (red elements are failed elements—snapshots taken at (a) peak load, (b) 1 in., and (c) 2 in. displacement points).
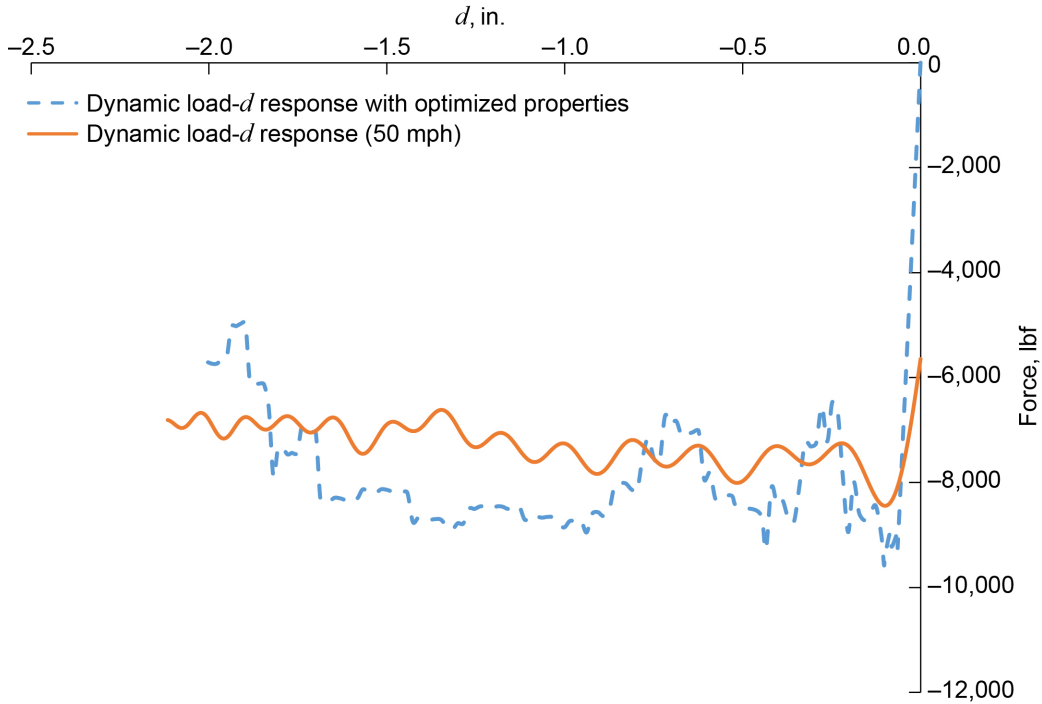

Figure 18.—Dynamic load-displacement (d) response of the corrugated panel compared with experiments.
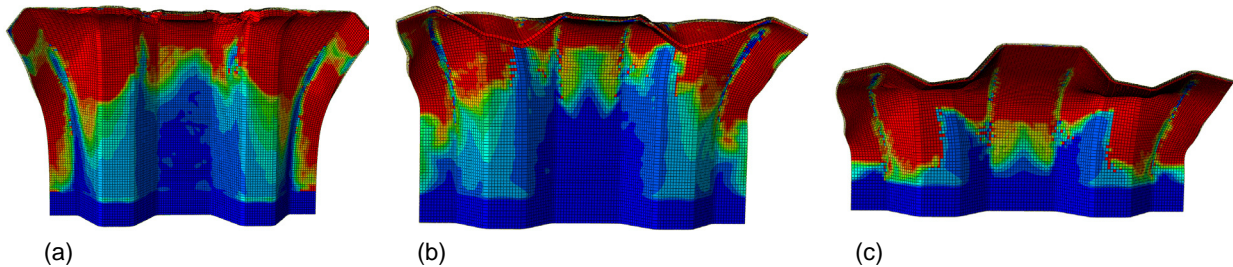

Figure 19.—Failure pattern of the corrugated panel (red elements are failed elements—snapshots taken at (a) peak load, (b) 1 in., and (c) 2 in. displacement points).

Conclusions

The predictive capability of the built-in Hashin progressive damage model in ABAQUS was successfully demonstrated on braided composite specimens (C-channel and corrugated) for a given quasi-static and dynamic crushing scenario. The model was initially calibrated, and model parameters were optimized through comparing the quasi-static load-displacement response of the C-shaped panel with experimental

results. Then, using the same model parameters, the quasi-static crushing response of the corrugated panel was *predicted* with results being in good agreement with experiments. The conducted parametric study on physical (experimentally measurable) and nonphysical (purely mathematical) model parameters revealed that by minor variation in model parameters, one can improve simulation results and gain a more in-depth understanding of the influence of model parameter variation on the crushing response of the composite.

Lessons learned:

- For a composite panel with a similar geometry, layup, and material properties, a 0.04 by 0.04 in. mesh size is adequate to achieve an accurate, converged, solution without compromising model efficiency.
- By defining proper boundary conditions at the base of the specimen itself, the base support can be removed from the model to reduce computational time without compromising accuracy. This also holds true in case of a dynamic impact, as long as the mass of the impactor is lower compared to the support mass. In dynamic cases where the impact mass is higher, a significant portion of the energy transmits into the support mass, and therefore, the support mass shall not be removed from the model.
- In order to gain a better understanding of the influence of model parameter variation on the crushing response of the composite, a small-scale parameter study was very helpful. For the composite damage model available in ABAQUS:
  1. Increasing/decreasing lamina strength has a notable impact on the peak crush load with some degree of influence on the post-peak slope.
  2. With higher/lower fracture toughness values, the mean post-peak crush load seems to be higher/lower, respectively. However, because of the highly nonlinear nature of the crushing mechanism in the post-peak region, most of the obtained load-displacement results lay in the "acceptable" range. Since there are no standardized test for measuring in-plane fracture toughness values, the parameter variation margin can be very wide. This gives the user more leverage on controlling the post-peak behavior of a given laminate.
  3. By default, the upper bound to all damage variables at a material point in ABAQUS is set to $d_{max} = 1$. This high value of d_{max} can cause solution instability and convergence problems. Although a completely damaged element is typically defined as an element with a $d_{max} \sim 1$, one can still lower the limit to a reasonable degree (~0.85) to avoid the instability caused by the default d_{max} definition in ABAQUS, and still preserve solution accuracy.
  4. Contact definitions (general vs. contact pairs) and loading curve slope (applied as smooth step) do not seem to have any notable impact on load-displacement results in the quasi-static crushing scenario.

Finally the predictive capability of the model was assessed using the available dynamic crush test results performed at the GRC Impact Lab. The same set of optimized model parameters was used to simulate the dynamic crushing response of both the C-channel and the corrugated panel, making both simulations "pure predictions" rather than calibrations. Reasonably good agreement was achieved for both panels considering the highly-nonlinear nature of the dynamic crushing scenario. Although further geometrical variations are required to fully assure the predictive capability of the model, this article demonstrates that with a short parametric study, one can achieve relatively reliable results with readily available engineering tools in ABAQUS.

References

1. Carruthers JJ, Kettle AP, Robinson AM. Energy absorption capability and crashworthiness of composite material structures: a review. Appl Mech Rev 1998;51:635–49.Metzger, J.W; "The behavior of ablating carbon phenolic", AIAA Paper 72-363, April, 1972

2. Farley GL, Jones RM. Crushing characteristics of continuous fiber-reinforced composite tubes. J Compos Mater 1992; 26(1):37–50.

3. Hinton MJ, Kaddour AS, Soden PD. A comparison of the predictive capabilities of current failure theories for composite laminates, judged against experimental evidence. Compos Sci Technol 2002;62(12–13):1725–97.

4. Feraboli P, Rassaian M. Proceedings of the CMH-17 (MIL-HDBK-17) Crashworthiness Working Group Numerical Round Robin. Costa Mesa, CA, July 2010.

5. Esnaola A, Elguezabal B, Aurrekoetxea J, Gallego I, Ulacia I. Optimization of the semi-hexagonal geometry of a composite crus structure by finite element analysis. Composites Part B 2016;93:56-66.

6. Bussadori BP, Schuffenhauer K, Scattina A. Modelling of CFRP crushing structures in explicit crash analysis. Composites: Part B 2014;60:725–735.

7. Azimi MB, Asgari M. A new bi-tubular conical circular structure for improving crushing behavior under axial and oblique impacts. International Journal of Mechanical Sciences 2016;105:253–265.

8. Ramos D. Master Thesis: Composite structures impact simulation behavior. Tecnico Lisboa. 2014.

9. Chiu LNS, Falzon BG Boman R, Chen B, Yan W. Finite element modelling of composite structures under crushing load. Composite Structures 2015;131:215–228.

10. El-Hage H, Mallick P K, Zamani N. Numerical modelling of quasi-static axial crush of square aluminum-composite hybrid tubes, International Journal of Crashworthiness, 2004; 9(6): 653-664, DOI: 10.1533/ijcr.2004.0320

11. Chien-Hua, HuangYa-Jung Lee. Experiments and simulation of the static contact crush of composite laminated plates. Composite Structures 2003;61(3):265-270

12. Naghipour P, Aktay L, Johnson A. Numerical investigation of structural crash response of thin-walled structures on soft soil. Materials and Design 2008; 29 (10):2052-2060.

13. Littell D, Jackson KE, Annett MS, Seal MD, Fasanella EL. The Development of Two Composite Energy Absorbers for Use in a Transport Rotorcraft Airframe Crash Testbed (TRACT 2) Full-Scale Crash Test. 71st AHS International Annual Forum and Technology Display; 5-7 May 2015; Virginia Beach, VA; United States. (ID:20160005978).

14. Feraboli P, Wade B, Deleo F, Rassaian M, Higgins M, Byar A. LS-DYNA MAT54 modeling of the axial crushing of a composite tape sinusoidal specimen. Composites: Part A, 2011;42:1809-25.

15. Wade B, Feraboli P, Rassaian M. LS-DYNA MAT54 modeling of the axial crushing of composite fabric channel and corrugated section specimens. Joint Advanced Materials & Structures Center of Excellence (JAMS) Technical Review. Crashworthiness and Aeroelasticity, 2014. Seattle, Washington.

16. LS-DYNA User's manual, Volume II Material Models. 2014 (LS-DYNA R7.1)

17. ABAQUS Analysis User's Guide 6.14. 2014.

18. Blanco N, Trias D, Pinho S.T, Robinson P. Intralaminar fracture toughness characterization of woven composite laminates. Part I: Design and analysis of a compact tension (CT) specimen. Engineering Fracture Mechanics 2014; 131: 349-360

19. Blanco N, Trias D, Pinho S.T, Robinson P. Intralaminar fracture toughness characterization of woven composite laminates. Part II: Experimental characterization. Engineering Fracture Mechanics 2014; 131: 361-370.